Identification of Severe Acute Respiratory Syndrome Coronavirus Replicase Products and Characterization of Papain-Like Protease Activity

Brian H. Harcourt,[1] Dalia Jukneliene,[2] Amornrat Kanjanahaluethai,[2,3] John Bechill,[2]
Kari M. Severson,[2] Catherine M. Smith,[2] Paul A. Rota,[1] and Susan C. Baker[2]*

*Centers for Disease Control and Prevention, Atlanta, Georgia[1]; Department of Microbiology and Immunology,
Stritch School of Medicine, Loyola University of Chicago, Maywood, Illinois[2]; and Department
of Microbiology, Faculty of Medicine, Chiang Mai University, Chiang Mai, Thailand[3]*

Gene 1 of the coronavirus associated with severe acute respiratory syndrome (SARS) encodes replicase polyproteins that are predicted to be processed into 16 nonstructural proteins (nsps 1 to 16) by two viral proteases, a papain-like protease (PLpro) and a 3C-like protease (3CLpro). Here, we identify SARS coronavirus amino-terminal replicase products nsp1, nsp2, and nsp3 and describe *trans*-cleavage assays that characterize the protease activity required to generate these products. We generated polyclonal antisera to glutathione S-transferase-replicase fusion proteins and used the antisera to detect replicase intermediates and products in pulse-chase experiments. We found that nsp1 (p20) is rapidly processed from the replicase polyprotein. In contrast, processing at the nsp2/3 site is less efficient, since a ≈300-kDa intermediate (NSP2-3) is detected, but ultimately nsp2 (p71) and nsp3 (p213) are generated. We found that SARS coronavirus replicase products can be detected by 4 h postinfection in the cytoplasm of infected cells and that nsps 1 to 3 colocalize with newly synthesized viral RNA in punctate, perinuclear sites consistent with their predicted role in viral RNA synthesis. To determine if PLpro is responsible for processing these products, we cloned and expressed the PLpro domain and the predicted substrates and established PLpro *trans*-cleavage assays. We found that the PLpro domain is sufficient for processing the predicted nsp1/2 and nsp2/3 sites. Interestingly, expression of an extended region of PLpro that includes the downstream hydrophobic domain was required for processing at the predicted nsp3/4 site. We found that the hydrophobic domain is inserted into membranes and that the lumenal domain is glycosylated at asparagine residues 2249 and 2252. Thus, the hydrophobic domain may anchor the replication complex to intracellular membranes. These studies revealed that PLpro can cleave in *trans* at the three predicted cleavage sites and that it requires membrane association to process the nsp3/4 cleavage site.

During the spring of 2003, in an unprecedented, rapid response to a mysterious respiratory illness, teams of scientists assembled by the World Health Organization identified a novel coronavirus as the cause of severe acute respiratory syndrome (SARS) (15, 16, 23, 24, 31). Coronaviruses are enveloped viruses that contain a large (27 to 32 kb) positive-strand RNA genome (reviewed in Lai and Holmes [17]). Currently, there are no effective vaccines or antiviral drugs to inhibit SARS coronavirus replication and pathogenesis. Therefore, the rapid identification of targets for the development of antiviral drugs is a high priority. Here, we describe the activity of one such target, the SARS coronavirus papain-like protease (PLpro), which is predicted to process the amino-terminal region of the replicase polyprotein during assembly of the viral replication complex.

SARS coronavirus replicates in the cytoplasm of the infected cell. The 5′-most 21 kb of the ≈29.7-kb viral genomic RNA is translated to produce two replicase polyproteins, termed pp1a and pp1ab (20, 24). pp1a is a ≈486-kDa polyprotein that is predicted to contain a papain-like protease (PLpro), a picornavirus 3C-like protease (3CLpro), two putative membrane proteins, MP1 (nsp4) and MP2 (nsp6), and several additional products of unknown function. pp1ab (≈790 kDa) is generated by ribosomal frameshifting and extends the pp1a product to include open reading frame (ORF) 1b, which contains the helicase domain (nsp13) (11) and predicted core RNA polymerase (nsp12), exonuclease (nsp14), endoribonuclease (nsp15), and methyltransferase (nsp16) activities (26). The pp1a and pp1ab polyproteins are predicted to be processed to generate 16 protein products (termed nonstructural proteins nsp1 to nsp16) which are predicted to assemble into a membrane-associated viral replication complex (28–30).

For the murine coronavirus mouse hepatitis virus, we showed that replicase products localize in double-membrane vesicles and that these vesicles are the sites of viral RNA synthesis (7). Furthermore, Kim and coworkers showed that the addition of cysteine protease inhibitor E64d to mouse hepatitis virus-infected cells blocked proteolytic processing and synthesis of viral RNA (14). Proteolytic processing of the coronavirus replicase polyproteins is essential for ongoing viral RNA synthesis. Therefore, the SARS coronavirus proteases are attractive targets for the development of antiviral drugs to reduce viral replication and pathogenicity. The structure and activity of the coronavirus 3CLpro have already been eluci-

* Corresponding author. Mailing address: Department of Microbiology and Immunology, Loyola University of Chicago, Stritch School of Medicine, 2160 South First Ave., Bldg. 105, Rm. 3929, Maywood, IL 60153. Phone: (708) 216-6910. Fax: (708) 216-9574. E-mail: sbaker1 @lumc.edu.

dated, and efforts to design inhibitors to 3CLpro are under way (1, 30, 32). Regarding SARS coronavirus PLpro, Thiel and coworkers demonstrated protease activity at the putative pp1a nsp2/3 cleavage site (30), but analysis of two other predicted cleavage sites and the identification of critical determinants recognized by this protease have not yet been done.

Here, we identify SARS coronavirus replicase products nsp1, nsp2, and nsp3 and describe *trans*-cleavage assays that characterize the protease activity required to generate these products. SARS coronavirus replicase products can be detected as early as 4 h postinfection and accumulate in punctate, perinuclear sites in infected cells. We found that PLpro cleaves the three predicted cleavage sites but with different kinetics and cofactors. We show that nsp1 (p20) is rapidly processed from the replicase polyprotein. In contrast, processing at the nsp2/3 site is less efficient, since a ≈300-kDa intermediate (NSP2-3) is detected, and the intermediate is ultimately processed to generate nsp2 (p71) and nsp3 (p213). By expressing the SARS coronavirus PLpro and the predicted substrates, we found that the PLpro domain alone is sufficient to process the predicted nsp1/2 and nsp2/3 sites. In contrast, we found that the expression of an extended region of PLpro that included the downstream hydrophobic domain was required for processing at the predicted nsp3/4 site. These results indicate that sequences downstream of the catalytic domain are important for facilitating PLpro-mediated processing at the nsp3/4 cleavage site.

MATERIALS AND METHODS

Virus and cells. The Urbani strain of SARS-associated coronavirus was used in all experiments (15). All work with infectious SARS coronavirus was performed inside a biosafety cabinet in the biosafety containment level 3 facilities at the Centers for Disease Control and Prevention, Atlanta, Ga. The SARS coronavirus was propagated in Vero E6 cells maintained in Dulbecco's modified Eagle's medium (DMEM) (Invitrogen, Grand Island, N.Y.) supplemented with penicillin and streptomycin (Invitrogen) and 10% heat-inactivated fetal bovine serum (HyClone, Logan, Utah).

The 50% tissue culture infectious dose ($TCID_{50}$) of the SARS coronavirus stock was determined by serially diluting the SARS coronavirus stock 1:10 per dilution and infecting eight wells per dilution of Vero E6 cells in a 96-well plate. Four days postinfection, the supernatant was removed, the cells were washed twice with phosphate-buffered saline (PBS) and stained with 2 ml of crystal violet working solution (stock solution: 10% formaldehyde, 1.3 g of crystal violet dissolved in 50 ml of methanol, in a final volume of 1 liter with distilled water; the stock solution is diluted 1:1 in PBS to generate the working solution) for 1 h. After staining, the cells were washed twice with PBS and allowed to air dry. The wells were inspected for virus-induced cytopathic effect and the $TCID_{50}$ was calculated with the Karber method (8).

Generation of SARS coronavirus antireplicase sera. Three regions (R1, amino acids 2 to 178; R2, amino acids 183 to 457; and R3, amino acids 1463 to 1746) were targeted for the development of antireplicase antisera (Fig. 1). The R1, R2, and R3 regions were generated by reverse transcription-PCR (RT-PCR) from SARS coronavirus RNA with the primers listed in Table 1, according to the manufacturer's instructions (Superscript RT-PCR for long templates; Invitrogen). The SARS coronavirus RNA was kindly provided to S.C.B. by the SARS Working Group at the Centers for Disease Control. PCR products were digested with appropriate restriction enzymes, ligated in-frame into the pGEX-5X-1 vector (Amersham Pharmacia Biotech), and transformed into *Escherichia coli*. The fusion proteins were induced, purified, and injected into rabbits for the generation of polyclonal antibodies as previously described (12, 25).

Radioimmunoprecipitation assays. Vero E6 cells (≈6 × 10⁴ cells/well in a six-well plate) were infected with ≈1.3 × 10⁴ $TCID_{50}$ of SARS coronavirus Urbani. For the pulse-chase experiments, the supernatant was removed at 20.5 h postinfection, the cells were washed once with PBS, and methionine-free DMEM (ICN Biomedicals, Inc., Aurora, Ohio) was added to the cells for 1 h. At 21.5 h postinfection, 100 μCi of ³⁵S-labeled methionine (ICN Biomedicals, Inc.) was added to each well for 30 min. At 22 h postinfection, the radiolabel was removed,

the cells were washed twice with PBS, and DMEM supplemented with penicillin and streptomycin and 10% heat-inactivated fetal bovine serum was added to the wells. One set of cells was immediately harvested as the time zero sample, and subsequently cells were harvested 30, 60, 90, and 120 min after the unlabeled chase was added. The cells were harvested by adding 300 μl of lysis buffer A (4% sodium dodecyl sulfate, 3% dithiothreitol, 40% glycerol, 0.065 M Tris-HCl, pH 6.8, and 0.01% bromophenol blue) to each well. The cells were then scraped together with a rubber policeman, and the lysate was passed through a 25-gauge needle to shear the DNA. The lysates were either used directly for immunoprecipitation assays or stored at −70°C for future studies.

To immunoprecipitate radiolabeled proteins, 50 μl of the cell lysate was diluted in 445 μl of radioimmunoprecipitation assay buffer (RIPA buffer: 0.5% Triton X-100, 0.1% sodium dodecyl sulfate [SDS], 300 mM NaCl, 4 mM EDTA, and 50 mM Tris-HCl, pH 7.4), 5 μl of the prebleed rabbit serum was added to clear the lysate, and the samples were incubated for 45 min at 4°C with rocking. Following incubation, 30 μl of GammaBind G Sepharose beads (Amersham Pharmacia Biotech AB, Uppsala, Sweden) were added to each sample and then rocked for 20 min at 4°C. The beads were then pelleted for 1 min at 5,000 rpm, and the supernatant was transferred to a new microcentrifuge tube. The designated antibody (5 μl) was added to each precleared lysate and then processed as described above. After pelleting the beads, the supernatant was removed, and the beads were washed twice with 500 μl of RIPA buffer and once with PBS. The beads were again pelleted, and 20 μl of lysis buffer A was added to each sample and incubated for 30 min at 37°C. The immunoprecipitated proteins were analyzed by electrophoresis on SDS-polyacrylamide gels. The gel was then fixed for 45 min in 10% methanol–10% acetic acid in water, treated with Amplify (Amersham Biosciences) for 30 min, dried, and exposed to X-ray film for 1 to 5 days.

Immunofluorescent staining. Vero E6 cells (≈4 × 10⁴ cells per chamber) were plated onto eight-chamber Falcon glass culture slides (Becton Dickinson, Franklin Lakes, N.J.). When the cells were approximately 80 to 90% confluent, the cells in each chamber were infected with 1,000 $TCID_{50}$ of SARS coronavirus Urbani. Cells were fixed, permeabilized, and stained at 4, 8, 11, 16, 20, and 24 h postinfection. For fixation and permeabilization of the cells, the medium was removed, the slides were washed once with PBS, fixed for 10 min with 2% paraformaldehyde, washed three times with PBS containing 10 mM glycine, and permeabilized for 10 min in PBS containing 0.1% Triton X-100. The cells were then washed three times with PBS containing 10 mM glycine, allowed to air dry, and either used immediately for indirect immunofluorescence assays or stored at −20°C.

To block nonspecific binding, the fixed cells were treated with blocking solution (1% bovine serum albumin, 0.5% fetal bovine serum, and 0.1% Tween 20 in PBS) for 30 min at room temperature. After removal of the blocking solution, 30 μl of anti-R3 serum (1:1,000 dilution in blocking solution) was added to each well and incubated for 30 min at room temperature in a humidified chamber. The cells were then washed three times for 1 min with blocking solution. Anti-rabbit immunoglobulin G (heavy and light chain) Alexa Fluor 488 secondary (Molecular Probes, Eugene, Oreg.) was diluted 1:500 in blocking solution, and 30 μl was added per well and incubated in the dark for 30 min at room temperature in a humidified chamber. The wells were washed three times for 1 min with blocking solution. For nuclear staining, 30 μl of propidium iodide (diluted 1:5,000 in blocking solution) was added to each well and incubated for 10 min. The slides were washed four times with PBS, allowed to air dry, and mounted with Dako fluorescent mounting medium (Dako Corporation, Carpinteria, Calif.) and coverslips. Cell staining was visualized with a Zeiss Axioskop with an Axiovert BlueH 485 filter, and pictures were taken with an RT Color Spot charge-coupled device camera (Diagnostic Instruments, Inc.).

BrUTP labeling and confocal microscopy. Newly synthesized viral RNA was labeled with 5-bromouridine 5'-triphosphate (BrUTP; Sigma, St Louis, Mo.) as previously described for mouse hepatitis virus infection (7). Briefly, Vero E6 cells were added to chamber slides, and when the cells were ≈60% confluent, they were mock infected or infected with 1,000 $TCID_{50}$ of SARS coronavirus and incubated in complete medium. At 20 h postinfection, 5 μg of actinomycin D (Sigma) per ml was added to the culture medium to block cellular RNA synthesis. At 21 h postinfection, cells were incubated for 1 h with 10 mM BrUTP and Lipofectamine (Invitrogen) according to the manufacturer's protocol for plasmid DNA transfection. Actinomycin D was present during the entire labeling period. Labeled RNA was visualized by indirect immunofluorescence detection with a mouse monoclonal antibody (anti-bromodeoxyuridine; Roche) and the secondary antibody goat anti-mouse-tetramethylrhodamine isothiocyanate (Jackson ImmunoResearch Laboratories). The cells were also incubated with anti-R1, anti-R2, or anti-R3 antibody and anti-rabbit immunoglobulin G (heavy and light chain) Alexa Fluor 488 secondary antibody to detect SARS coronavirus replicase products.
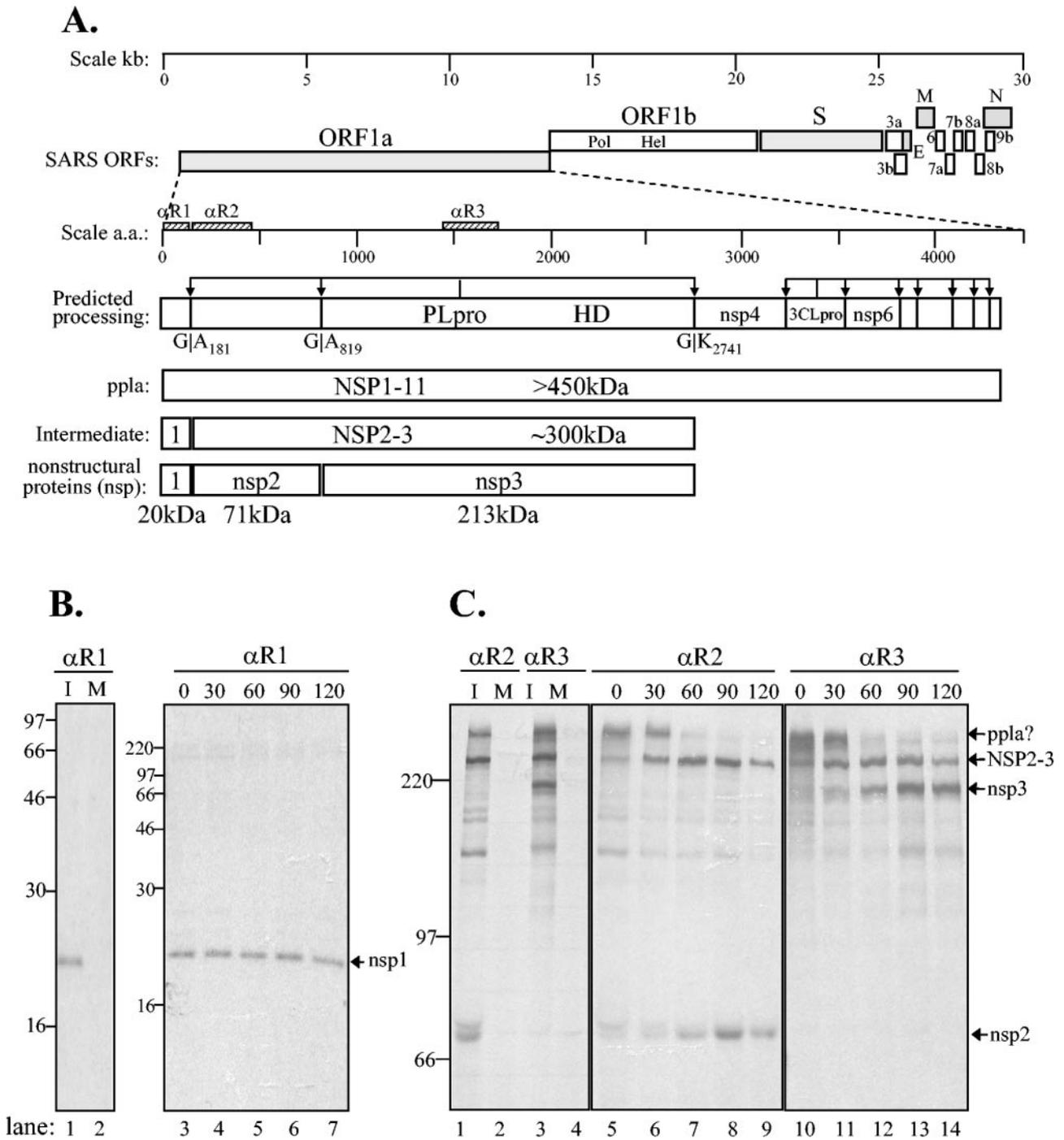
FIG. 1. Identification of SARS coronavirus ORF1a intermediate NSP2-3 and products nsp1, nsp2, and nsp3 by pulse-chase analysis. (A) Schematic diagram illustrating the SARS coronavirus open reading frames (ORFs), the predicted processing of polyprotein 1a (pp1a) to nonstructural protein (nsp) products, and regions used to generate anti-R1, anti-R2, and anti-R3 sera. The papain-like proteinase domain (PLpro), hydrophobic domain (HD), and picornavirus 3C-like proteinase domain (3CLpro) are designated. (B) Detection of nsp1 by immunoprecipitation with anti-R1 serum from SARS coronavirus-infected (I) and mock-infected (M) cells radiolabeled with [^{35}S]methionine for 60 min from 21 to 22 h postinfection. For the pulse-chase analysis, SARS coronavirus-infected Vero E6 cells were pulse-labeled with [^{35}S]methionine from 21.5 to 22.0 h postinfection. The labeling medium was then replaced with complete DMEM. Cells were lysed at the chase times indicated in lanes 3 to 7, and total lysates were subjected to immunoprecipitation with anti-R1 serum. Products were analyzed on an SDS–12.0% polyacrylamide gel and subjected to autoradiography. (C) Detection of NSP2-3 intermediate and processed products nsp2 and nsp3 by immunoprecipitation with anti-R2 and anti-R3 sera. SARS coronavirus-infected, radiolabeled cell lysates were prepared as above, and products were analyzed on an SDS–8.0% polyacrylamide gel and subjected to autoradiography. The positions of molecular size markers are shown on the left of each gel (in kilodaltons).

TABLE 1. Primers used for amplification or mutagenesis of SARS coronavirus sequences

Purpose	Primer	Oligonucleotide sequence (5′ to 3′)[a]	Nucleotides	Polarity or change
Generation of GST-R1 fusion protein	S-5	TTGAATTCGAGAGCCTTGTTCTTGGTG	268–286	Forward
	S-6	TTCTCGAGATTGAGCTCACGAGTGAG	781–795	Reverse
Generation of GST-R2 fusion protein	S-9	TTGGATCCTCACTCGCTATGTCGACAAC	809–829	Forward
	S-10	TTCTCGAGTTCACGACTCAGTATCTC	1618–1635	Reverse
Generation of GST-R3 fusion protein	S-3	TTGAATTCAATGGATACCTCACTTC	4651–4667	Forward
	S-4	AACTCGAGCATCACAGCTTCTACAC	5486–5502	Reverse
Generation of pPLpro-HD expression construct	SR-1	AAGGATCCGCCATGGAACAAAAACTCATATCAGAAG		Forward
	SR-2	CTCATATCAGAAGAGGATCTGCGGGAGGTTAAGACTATAAA	4882–5001	Forward
	SR-4	TAGAATTCTTGTGAGTCTTGCAGAAGCC	7522–7541	Reverse
Generation of pPLpro expression construct	SR-49	AAGGATCCACTATGGAGGTTAAGACTATAAAAG	4884–5003	Forward
	SR-50	GGCTCGAGAACAATTTAGAAAATTTGGGTGA	6853–6876	Reverse
Generation of pNSP1-3∗ expression construct	SR-47	GAGGATCCCCTTGTTCTTGGTGTCAACGAG	273–294	Forward
	SR-48	CCGAATTCCACATAGCGATTGTGAAC	6873–6891	Reverse
	SR-60	GGAAGCTTACCATGGATTACAAGGATGAC		Forward
	SR-61	CCGAATTCCGAACCGTCTGCACGCACAC	3688–3707	Reverse
Generation of pNSP∗ 3-4 expression construct	SR-51	CCGGATCCATCATGGATGGTTGCACCTC	7393–7412	Forward
	SR-3	TAGAATTCAGAACAGCAGAAGTGATTGATG	9959–9981	Reverse
Generation of EGFP-HD expression construct	SR-110	TTCTCGAGCTAAATTGTTCACAATCG	6866–6883	Forward
	SR-111	TTGGATCCCCATATGTAGTAGAAAGAAGC	7357–7377	Reverse
Site-directed mutagenesis[b] of pPLpro-HD	SR-6	GGGCTGATAACAATGCTTATTTGTCTAGTG	5201–5230	C1651A
	SR-8	CTGCTAACTTTGCTGCACTCATACTCGC	5315–5342	C1688A
	SR-35	GGTAACTATCAGTGTGGTGCTTACACTCATATAAC	5680–5714	H1812A
	SR-37	GTGTGGTCATTACACTGCTATAACTGCTAAGGAG	5691–5724	H1815A
	SR-39	GAGAATTGTATCTTGCTTCGTCTAACGTTACTAC	6995–7028	N2249A
	SR-41	TATCTTAATTCGTCTGCCGTTACTACTATGG	7003–7033	N2251A
Site-directed mutagenesis of pNSP∗3-4	SR-20	CTCACTCAAGGGTGCTAAGATTGTTAGTACTT	8469–8500	G2740A

[a] Underlined nucleotides were added for cloning purposes or mutated sequences.
[b] The sequence of one primer of each complementary primer pair is shown.

Confocal microscopy was performed with a Zeiss LSM 510 laser-scanning confocal microscope equipped with an argon laser and an HeNe laser and appropriate filters. The thickness of each digital section obtained by the microscope was 1.5 µm. Approximately 100 cells were examined to ensure that the results were representative. Image analysis was performed with the standard system-operating software provided with the microscope. Fluorescent images were superimposed digitally to allow fine comparison. Colocalization of green (Alexa Fluor 488) and red (tetramethylrhodamine isothiocyanate) signals in a single pixel produce yellow, while separated signals remain green or red.

Generating SARS pPLpro and substrate expression constructs and site-directed mutations. Constructs expressing the SARS coronavirus replicase coding regions were generated with specific primers (Table 1) to reverse transcribe and PCR amplify the designated region from RNA isolated from SARS coronavirus-infected cells. RT-PCRs were performed with Superscript One-step RT-PCR for long templates according to the manufacturer's instructions (Invitrogen). For some constructs, a second round of PCR was performed to add an ATG start codon and an epitope tag to the amino-terminal end of the construct. The amplified products were then digested with appropriate restriction enzymes and ligated into the corresponding sites in the pcDNA3.1/V5-His expression vector version B (Stratagene, La Jolla, Calif.). The ligated DNA was transformed into *E. coli* XL-1 Blue competent cells according to the manufacturer's instructions (Stratagene), except that the bacteria were grown at 25°C. To generate specific mutations in the catalytic domain or substrate cleavage sites, mutagenic primers (Table 1) were incorporated into newly synthesized DNA with the QuikChange site-directed mutagenesis protocol (Stratagene, La Jolla, Calif.) and as previously described (12). All introduced mutations were confirmed by DNA sequencing.

SARS coronavirus PLpro *trans*-cleavage assays. SARS coronavirus PLpro and substrates cloned into plasmids under T7 promoter control were cotransfected into HeLa-MHVR cells infected with recombinant vaccinia virus expressing the bacteriophage T7 polymerase as previously described (12). Briefly, newly synthesized proteins were metabolically labeled with 50 uCi of Trans35S-label (ICN, Costa Mesa, Calif.) per ml from 5.5 to 10.5 h postinfection. Cells were washed in PBS, and cell lysates were prepared by scraping the cells in 300 µl of lysis buffer A. The cell lysate (50 µl) was diluted in 1.0 ml of RIPA buffer and subjected to immunoprecipitation with anti-V5 antibody (Invitrogen, Carlsbad, Calif.) and protein A-Sepharose beads (Amersham Bioscience, Piscataway, N.J.). The immunoprecipitated products were analyzed by electrophoresis on a 5.0 to 12.5% polyacrylamide gel containing 0.1% sodium dodecyl sulfate. Following electrophoresis, the gel was fixed in 25% meth-anol–10% acetic acid, enhanced with Amplify (Amersham Biosciences) for 60 min, dried, and exposed to Kodak X-ray film at −70°C.

In vitro transcription and translation. The TNT T7-coupled reticulocyte lysate system (Promega, Madison, Wis.) was used according to the manufacturer's instructions. In vitro transcription and translation was performed for 90 min at 30°C in the presence of 0.8 uCi of Trans-35S label per ml in a volume of 25 µl. Where indicated, 1.0 µl of canine pancreatic microsomes (Promega) was added prior to the incubation. For analyses of membrane association, the products of in vitro transcription and translation were subjected to high-speed centrifugation (15,000 rpm in an Eppendorf microcentrifuge for 10 min). The supernatant was removed, the pellet (which may contain aggregated or membrane-associated proteins) was resuspended in lysis buffer A, and both fractions were analyzed by SDS-polyacrylamide gel electrophoresis (PAGE).

Endoglycosidase H treatment. For endoglycosidase H treatment, lysates from vTF7.3-infected and pPLpro-HD-transfected cells were prepared and subjected to immunoprecipitation as described above. Protein A-Sepharose-antibody-antigen complexes were washed once in RIPA buffer, and endoglycosidase H treatment was performed as suggested by the manufacturer (Roche, Indianapolis, Ind.). Briefly, the complexes were resuspended in 20 µl of 50 mM sodium phosphate buffer, pH 6.0, and incubated in the presence or absence of a final concentration of 1 unit of endoglycosidase H per microliter for 16 h at 37°C. Following the incubation, an equal volume (25 µl) of lysis buffer A was added to each sample, mixed, and incubated for 30 min at 37°C. The Sepharose beads were pelleted by a brief, high-speed spin in a microcentrifuge, and the supernatant was loaded directly for analysis by SDS-PAGE.

Expression of EGFP and EGFP-HD. The hydrophobic domain (HD) region of nsp3 was PCR amplified from pPLproHD with primers SR-110 and SR-111 (Table 1), cloned into the expression vector for eukaryotic green fluorescent protein (EGFP), pEGFP (BD Biosciences), and designated pEGFP-HD. The pEGFP and pEGFP-HD DNAs were transfected into HeLa cells with Lipofectamine (Invitrogen) according to the manufacturer's instructions, and the protein product was detected by confocal microscopy as described above.

RESULTS

Identification of SARS coronavirus ORF1a intermediates and products. The SARS coronavirus replicase polyproteins

pp1a and pp1ab are predicted to be processed into 16 nonstructural proteins by two distinct proteases, PLpro and 3CLpro (28, 30). Because proteolytic processing is required for coronavirus RNA synthesis (14), these proteases are attractive targets for the development of antiviral drugs. As a first step toward characterizing one of these proteases, we focused on PLpro and identified the replicase products processed by this protease in virus-infected cells and developed *trans*-cleavage assays to assess PLpro activity.

To identify the replicase products cleaved by PLpro, we generated rabbit polyclonal anti-R1, anti-R2, and anti-R3 antibodies to the three predicted amino-terminal cleavage products nsp1, nsp2, and nsp3 (Fig. 1 and Table 1) as described in Materials and Methods. We then used these antisera to immunoprecipitate SARS coronavirus replicase intermediates and products from radiolabeled infected cells. Our previous studies of mouse hepatitis virus replicase processing demonstrated that intermediates and products can be detected by pulse-chase analysis (7, 25). Therefore, we pulse-labeled SARS coronavirus-infected cells for 30 min and then removed the radiolabel and chased with unlabeled medium for 30 to 120 min. Cells were labeled from 20 to 20.5 h postinfection, a time when >90% of the cells were infected and expressing replicase products, as indicated by immunofluorescence studies (shown in Fig. 2).

With the anti-R1 serum directed against the amino-terminal replicase domain, we identified nsp1 as a ≈20-kDa protein that was detected from the pulse-labeled lysates and stable throughout the 120-min chase period (Fig. 1B). No specific proteins were immunoprecipitated from mock-infected cells with the anti-R1 serum (lane 2) or from SARS coronavirus-infected cells with the preimmune serum (data not shown). The 20-kDa protein detected in SARS coronavirus-infected cells by anti-R1 is consistent with the size of the product expected if PLpro cleaves the replicase pp1a at the glycine-180/alanine-181 cleavage site (28, 30). No precursor was detected, suggesting that nsp1 is rapidly processed from the pp1a polyprotein.

In contrast to the rapid processing of nsp1, we found that processing at the nsp2/3 cleavage site occurs more slowly, since an intermediate of ≈300 kDa is detected with both anti-R2 and anti-R3 sera (Fig. 1C, lanes 1, 3, and 5 to 14). The NSP2-3 intermediate is ultimately processed into nsp2 (≈71 kDa), which was detected with anti-R2 serum (Fig. 1C, lane 1 and 5 to 9), and nsp3 (≈213 kDa), which was detected with anti-R3 serum (Fig. 1C, lanes 3 and 10 to 14). Processing of the NSP2-3 intermediate was apparent by 60 min of chase and continued at 90 and 120 min. The sizes of the nsp2 and nsp3 proteins are consistent with the expected sizes of the products if processing occurs at the predicted glycine-818/alanine-819 and glycine-2740/lysine-2741 PLpro cleavage sites (28, 30). Overall, we were able to use the antireplicase antisera to identify nsp1, nsp2, and nsp3 final products and the NSP2-3 intermediate from SARS coronavirus-infected cells.

Previous studies with mouse hepatitis virus have shown that coronavirus replicase proteins localize in punctate, perinuclear sites in the cytoplasm of virus-infected cells (5, 7, 25). To determine where SARS coronavirus replicase products localized, we performed immunofluorescence studies and colocalization experiments. First, we looked at the expression and localization of replicase proteins in SARS coronavirus-infected

Vero E6 cells (Fig. 2). We found that replicase products could be detected as early as 4 h postinfection (Fig. 2B) and that the number of infected cells increased throughout the 24-h time course (Fig. 2B to G), likely from the spread of infectious virus from the initially infected cells. By 20 to 24 h postinfection, all the cells were infected and expressing viral replicase products, as shown by staining with anti-R3 antibody (Fig. 2F and G). The SARS coronavirus infection spread throughout the monolayer, although there was no obvious syncytium formation. Immunofluorescent staining experiments with anti-R1 and anti-R2 antibodies revealed a very similar pattern of punctate, perinuclear localization, as shown by confocal microscopy in Fig. 3E and H. The time course and spread of viral infection shown here are in agreement with studies that used electron microscopy to monitor SARS coronavirus replication from 1 to 30 h postinfection in Vero cells (21).

To determine if the nonstructural proteins are detected at the sites of viral RNA synthesis, we performed colocalization experiments. Previously, we showed that newly synthesized coronavirus RNA could be visualized after incorporation of BrUTP and indirect immunofluorescent staining with a monoclonal antibody that recognizes bromodeoxyuridine-containing RNA (27). These previous studies showed that mouse hepatitis virus RNA colocalized with replicase products in double-membrane vesicles, which are the site of replication for nidoviruses such as mouse hepatitis virus and equine arteritis virus (7, 22). To determine if the amino-terminal replicase products colocalized with sites of viral RNA synthesis, we treated SARS coronavirus-infected cells with actinomycin D to block host cell mRNA synthesis and transfected the cells with BrUTP to label newly synthesized viral RNA as described in Materials and Methods.

The cells were fixed and stained with anti-R1, anti-R2, or anti-R3 antibody to detect SARS coronavirus replicase products or antibromodeoxyuridine antibody to detect newly synthesized viral RNA and visualized by confocal microscopy (Fig. 3). We found that the punctate, perinuclear staining of the viral replicase products colocalized with the sites of SARS coronavirus RNA synthesis as detected by staining with antibromodeoxyuridine antibody (Fig. 3, overlay). For the cells stained with anti-R3, we show the highly punctate staining typically detected early in infection. For the cells stained with anti-R2, we show the more intense, perinuclear staining detected later in infection, when replicase products accumulate in the cytoplasm of the cell. For the cells stained with anti-R1, we note that the majority of the areas that are positive for nsp1 are also positive for newly synthesized viral RNA. However, nsp1 is not detected at all sites of RNA synthesis, which may indicate low levels of protein that cannot be detected by our antibody or that nsp1 is only transiently associated with RNA synthesis.

Overall, these experiments indicate that viral nsp1, nsp2, and nsp3 are intimately associated with the viral RNA replication machinery, the membrane-associated viral replication complex. These results are consistent with recent electron microscopy studies that identified double-membrane vesicles in the cytoplasm of SARS coronavirus-infected cells (6). These membranous structures were also detected in a bronchial alveolar lavage specimen from a patient with SARS (6). Our results indicate that the amino-terminal replicase intermediates and/
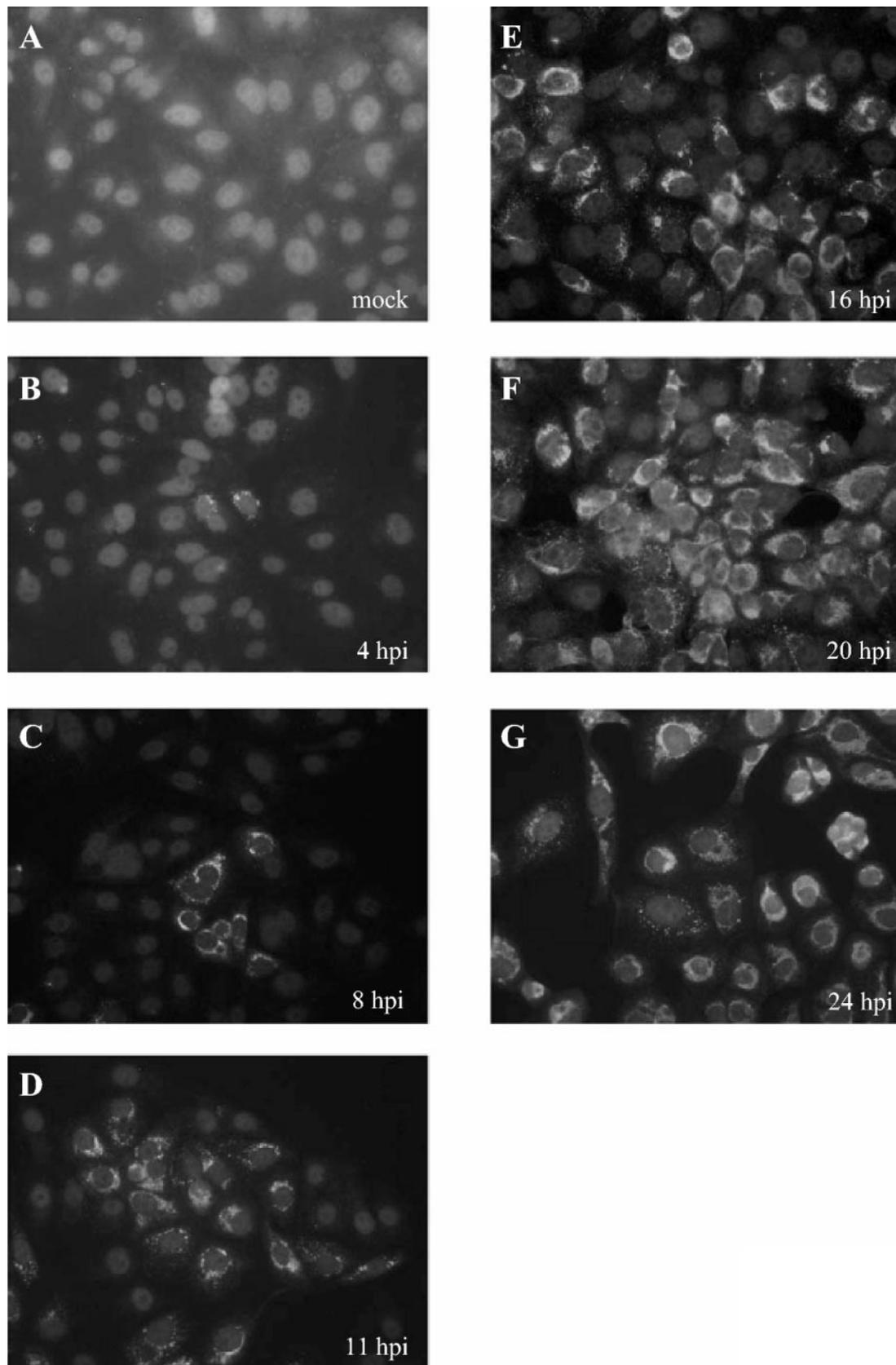
FIG. 2. Detection of SARS coronavirus replicase products by indirect immunofluorescent staining. Vero E6 cells were infected with 1,000 $TCID_{50}$ of SARS coronavirus Urbani, fixed and permeabilized at 4, 8, 11, 16, 20, or 24 h postinfection, and stained with anti-R3 and fluorescein isothiocyanate-conjugated anti-rabbit immunoglobulin as described in Materials and Methods.
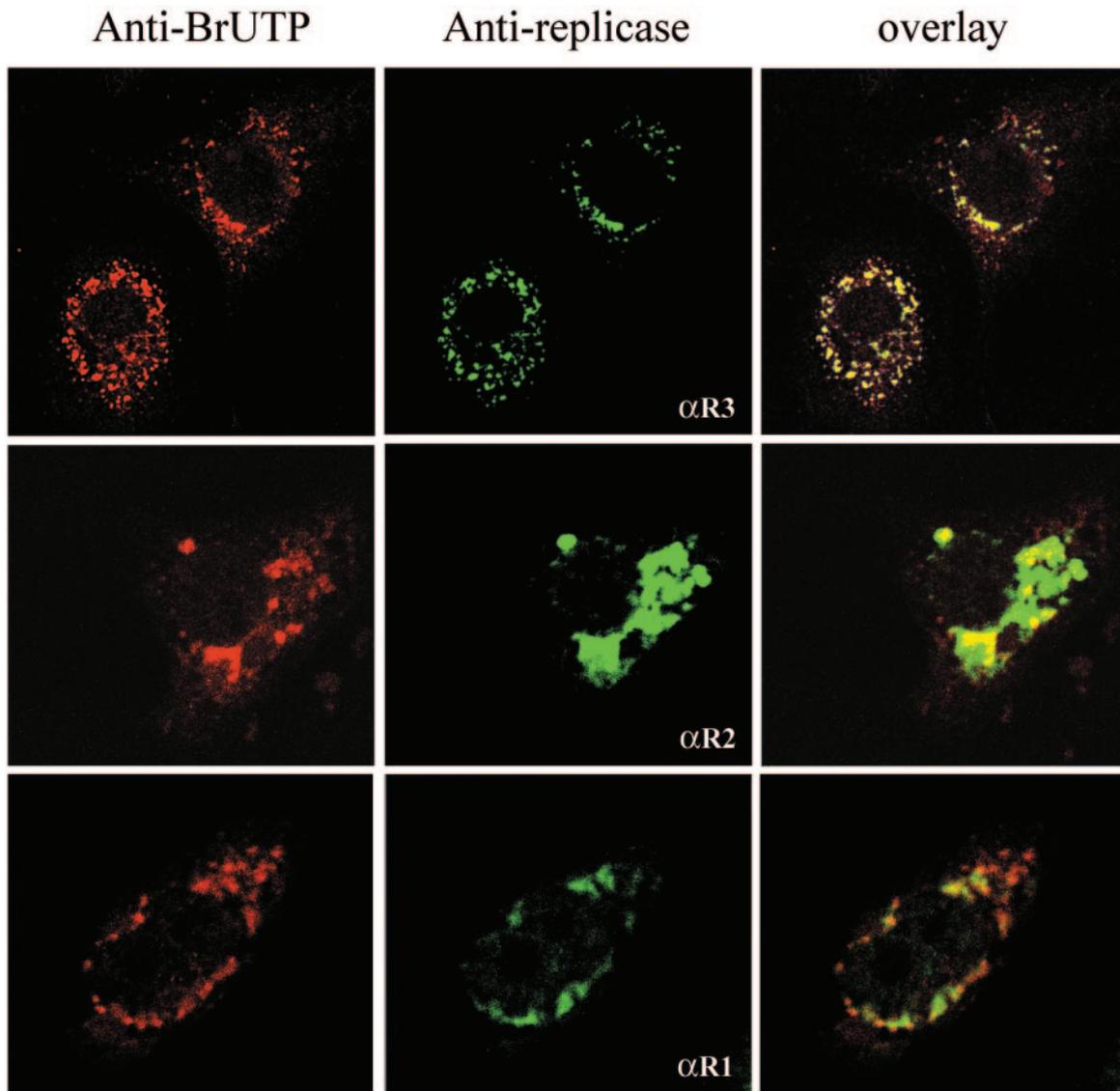
FIG. 3. Colocalization of SARS coronavirus replicase products with de novo-synthesized viral RNA. SARS coronavirus-infected cells were transfected with Lipofectamine containing BrUTP at 21 h postinfection. Cells were treated with actinomycin D (5 μg/ml) to block cellular mRNA synthesis. The cells were double stained with rabbit polyclonal antisera against nsp1 (anti-R1), nsp2 (anti-R2), or nsp3 (anti-R3) and a mouse monoclonal antibromodeoxyuridine antibody to detect newly synthesized RNA.

or processed products assemble as part of the membrane-associated viral replication complex that mediates SARS coronavirus RNA synthesis.

Characterizing SARS coronavirus PLpro activity with *trans*-cleavage assays. SARS coronavirus PLpro was proposed to process the amino-terminal end of the pp1a polyprotein at three sites: glycine-180/alanine-181 (nsp1/2 cleavage site), glycine-818/alanine-819 (nsp2/3 cleavage site), and glycine-2740/lysine-2741 (nsp3/4 cleavage site) (28, 30) (Fig. 1). In vitro transcription and translation studies provided evidence of PLpro-mediated processing at the glycine-818/alanine-819 cleavage site (30), but PLpro-mediated processing at the other putative cleavage sites has not been experimentally confirmed.

To establish an assay for SARS coronavirus PLpro activity, we cloned and expressed the PLpro domain (termed PLpro, amino acid residues 1541 to 2204) and a substrate encompass-

ing both the nsp1/2 and nsp2/3 cleavage sites (termed NSP1-3*, amino acid residues 4 to 1148). The targeted domains were amplified by RT-PCR from SARS coronavirus-infected cell RNA with the primers listed in Table 1 and ligated into a pcDNA expression vector as described in Materials and Methods and diagrammed in Fig. 4A. A *trans*-cleavage assay was performed by cotransfection of plasmids encoding pPLpro and pNSP1-3* into cells infected with vaccinia virus expressing T7 polymerase. Newly synthesized proteins were radiolabeled with Trans^{35}S label for 5 h, cells were lysed, and the lysates were subjected to immunoprecipitation with anti-R1, anti-R2, or anti-V5 antibodies (Fig. 4B).

PLpro mediated processing of the NSP1-3* substrate, releasing nsp1 (Fig. 4B, lane 3), nsp2 (Fig. 4B, lane 6), and the truncated product nsp3* (Fig. 4B, lane 9). In addition, we identified a putative intermediate in processing, NSP2-3*, that
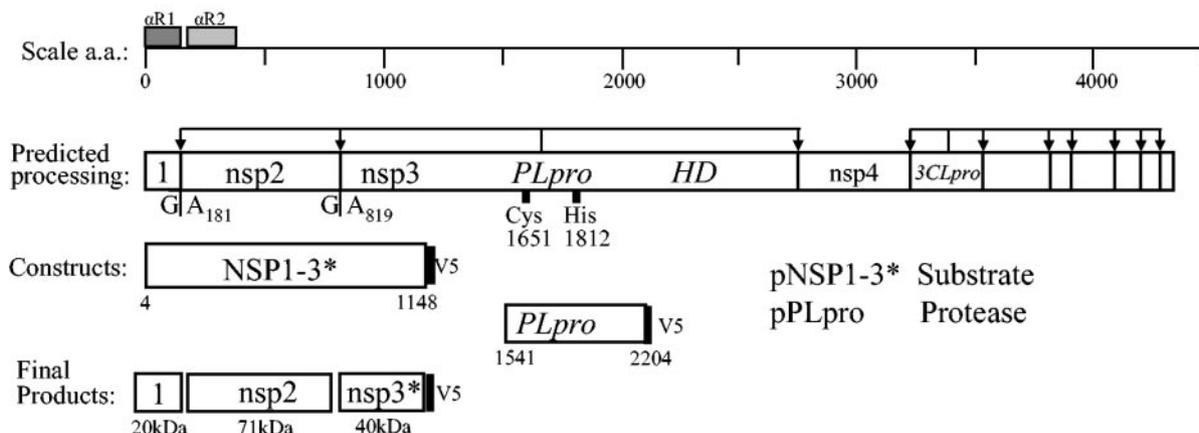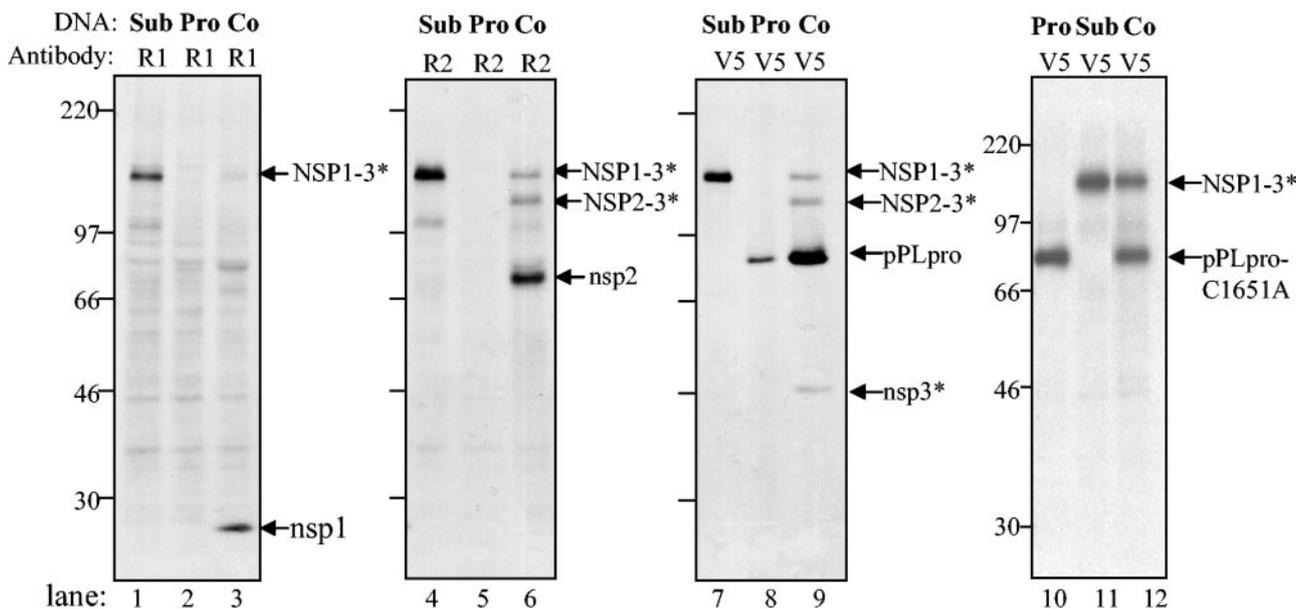
FIG. 4. Analysis of products expressed from SARS coronavirus pPLpro and pNSP1-3* constructs alone and during coexpression in a *trans*-cleavage assay. (A) Schematic diagram of the predicted processing of SARS coronavirus ORF1a, the constructs expressing the NSP1-3* substrate and PLpro, and the expected final products. (B) Detection of processing by PLpro of the nsp1/2 and nsp2/3 cleavage sites in ORF1a. HeLa-MHVR cells were infected with vTF7.3 and transfected with plasmid DNAs as indicated above each lane. Newly synthesized proteins were labeled with Trans^{35}S label from 5.5 to 10.5 h postinfection. Lysates were prepared and subjected to immunoprecipitation with anti-R1, anti-R2, or anti-V5 antibody. Immunoprecipitated proteins were analyzed by electrophoresis on an SDS–5.0 to 12.5% polyacrylamide gel, processed, and subjected to autoradiography. Products were immunoprecipitated with anti-R1, anti-R2, or anti-V5 epitope tag antibody from cells transfected with DNA encoding the SARS coronavirus NSP1-3* substrate region alone (lanes 1, 4, and 7), the SARS coronavirus PLpro alone (lanes 2, 5, and 8), or cotransfected with both constructs (lanes 3, 6, and 9) or an inactive mutant of PLpro (lane 12). The positions of molecular size markers are shown on the left of each gel (in kilodaltons).

is detected with anti-R2 and anti-V5 antibodies (Fig. 4B, lanes 6 and 9). These results demonstrate that the PLpro domain can act in *trans* to process the amino-terminal end of the pp1a polyprotein. To verify that the PLpro catalytic domain was required for protease activity, we performed site-directed mutagenesis and changed the catalytic cysteine-1651 to alanine, a substitution that has been shown previously to abolish PLpro activity (30). As expected, we found that PLproC1651A was unable to process NSP1-3* (Fig. 4B, lane 12).

To determine if PLpro mediates processing at the downstream nsp3/4 cleavage site, we generated a substrate expression construct, designated pNSP*3-4, that contained the C-terminal region of nsp3 and extended to residue 3239 of nsp4 (Fig. 5A). This substrate was cotransfected with either PLpro or an extended version of PLpro that encompassed the downstream hydrophobic domain (pPLpro-HD). Interestingly, we found that PLpro was insufficient to mediate processing at the nsp3/4 cleavage site (Fig. 5B, lane 5). However, PLpro-HD

A.

B.

C.
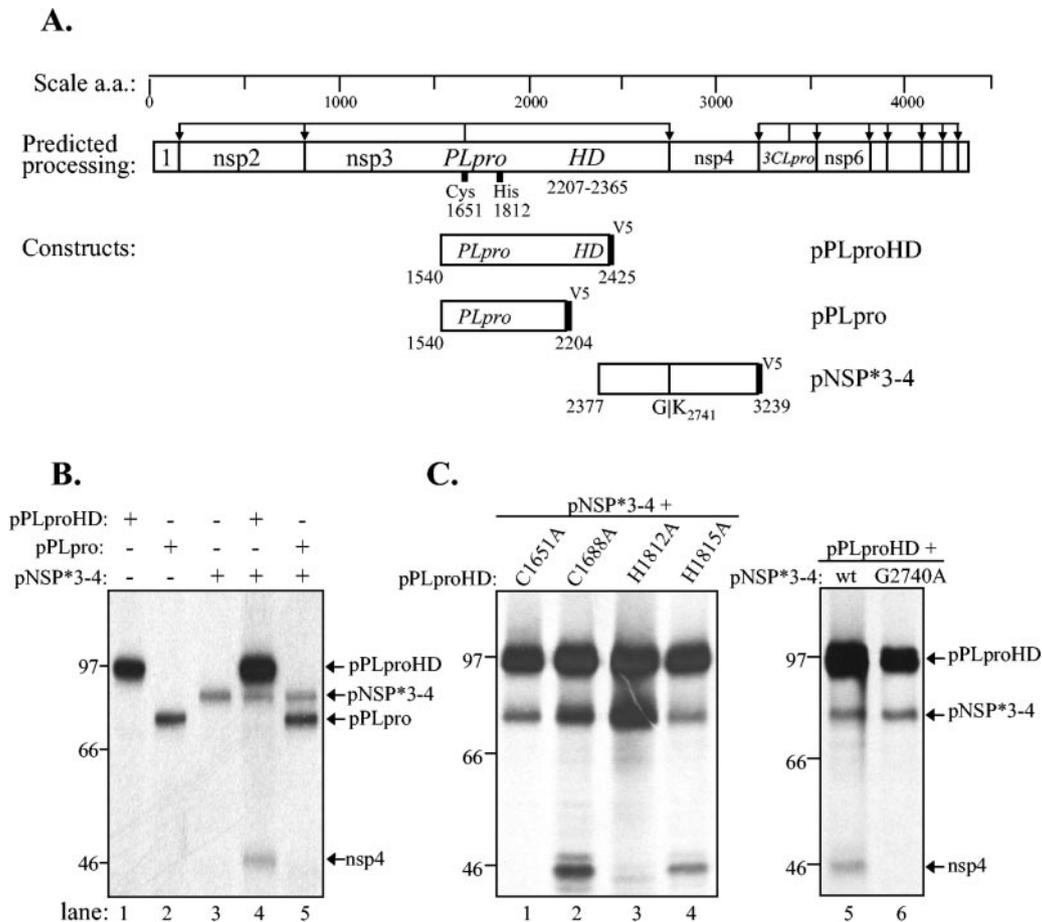
FIG. 5. Analysis of products expressed from SARS coronavirus pPLpro-HD, pPLpro, and pNSP*3-4 constructs alone and during cotransfection in a *trans*-cleavage assay. (A) Schematic diagram of the predicted processing of SARS coronavirus ORF1a, the constructs expressing PLpro, PLpro-HD, and the NSP*3-4 substrate. (B) Detection of processing by PLpro-HD at the nsp3/4 cleavage site of ORF1a. The *trans*-cleavage assay was performed as described for Fig. 4 and in Materials and Methods. (C) Effect of amino acid substitutions on PLpro activity. Predicted catalytic and control residues (indicated above the lanes) were changed to alanine, plasmid DNA was cotransfected with pNSP*3-4, and products were analyzed by SDS-PAGE (lanes 1 to 4). The effect of changing glycine to alanine in the P1 position of the nsp3/4 cleavage site is shown in lane 6. The positions of molecular size markers are shown on the left of each gel (in kilodaltons).

processed the NSP*3-4 substrate, as shown by the release of the cleavage product nsp4 (Fig. 5B, lane 4). Predicted catalytic residues cysteine-1651 and histidine-1812 are required for processing, because substitution of these residues to alanine abolishes activity (Fig. 5C, lanes 1 and 3).

To determine if this processing is indeed occurring at the predicted nsp3/4 cleavage site, we performed site-directed mutagenesis and changed glycine-2740 to alanine. As expected, this mutant substrate was not processed by PLpro-HD (Fig. 5C, lane 6), since a glycine at the P1 position of the cleavage site is generally required for coronavirus papain-like protease-mediated processing (13, 19). These *trans*-cleavage assays revealed a significant difference in the ability of PLpro to process the upstream cleavage sites (nsp1/2 and nsp2/3) and the downstream cleavage site (nsp3/4). Processing at the downstream cleavage site required expression on PLpro-HD, suggesting that membrane association may be important for processing at the nsp3/4 site or that the hydrophobic domain may modulate PLpro activity.

The designation hydrophobic domain refers to the fact that this region (amino acid residues 2207 to 2365) contains

stretches of predominantly hydrophobic amino acids that may serve to anchor nsp3 to intracellular membranes (Fig. 6A). To determine if the HD mediates membrane association and if the NSP*3-4 substrate is membrane associated, we performed in vitro transcription and translation experiments in the presence and absence of canine microsomal membranes and determined if the translated products became membrane associated. After translation, the products were subjected to high-speed centrifugation to separate the soluble proteins and proteins that pellet due to aggregation or membrane association. The soluble and pellet fractions were analyzed by SDS-PAGE and visualized by autoradiography.

As expected, in the absence of canine microsomal membranes, PLpro-HD and NPS*3-4 remain soluble (Fig. 6B, CMM−). However, in the presence of canine microsomal membranes, 60% of PLpro-HD and 47% of NPP*3-4 were associated with the membranous pellet (Fig. 6B, CMM+). In addition, the membrane-associated PLpro-HD product migrated more slowly than the protein from the soluble fraction, suggesting that it was modified after membrane association.

While scanning the HD amino acid sequence, we identified

A.　　　　　SARS-CoV nsp3 Hydrophobic Domain

2200　FSKLFTIAMWLLLLSICLGSLICVTAAFGVLLSNFGAPSYCNGVR

　　　　　　*　*
2245　ELYLNSSNVTTMDFCEGSFPCSICLSGLDSLDSYPALETIQVTIS

2290　SYKLDLTILGLAAEWVLAYMLFTKFFYLLGLSAIMQVFFGYFASH

2335　FISNSWLMWFIISIVQMAPVSAMVRMYIFFASFYYIWKSYVHIMD
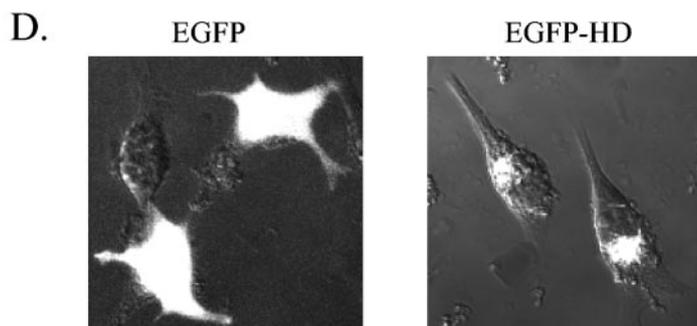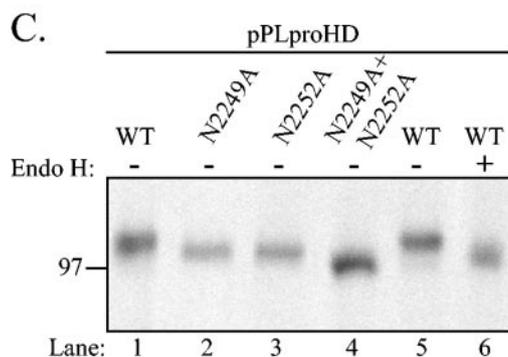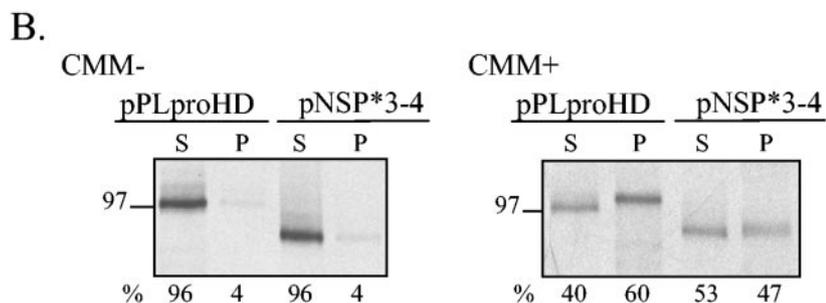
FIG. 6. Membrane association of PLpro-HD and NSP*3-4 proteins and N-linked glycosylation of asparagine residues in the hydrophobic domain. (A) Sequence of the SARS coronavirus nsp3 hydrophobic domain (HD, amino acid residues 2207 to 2365). Consensus sites for N-linked glycosylation are indicated by *. Underlined amino acid residues are potential transmembrane sequences (bioinformatics analysis with www.expasy .org). (B) Detection of membrane association of the PLpro-HD and NSP*3-4 substrate. Plasmid DNAs were linearized and subjected to in vitro transcription and translation in the absence or presence of canine microsomal membranes (CMM). Proteins were labeled with Trans-^{35}S label, immunoprecipitated with anti-V5 antibody, analyzed by electrophoresis on SDS–10% polyacrylamide gels, visualized by autoradiography, and quantitated by phosphorimaging. The percentage of total protein detected in the soluble (S) versus the pelleted (P) fraction is indicated below the gel. (C) Effect of amino acid substitution of asparagine residues 2249 and 2252 on the migration of the PLpro-HD protein. Asparagine residues were changed to alanine residues by site-directed mutagenesis as described in Materials and Methods. Wild-type and mutant plasmid DNAs were expressed via the vaccinia virus-T7 expression system, and immunoprecipitated products were analyzed by electrophoresis on SDS–10% poly-acrylamide gels. The effect of treatment with endoglycosidase H (Endo H) to remove N-linked glycosylation is shown in lane 6. (D) Detection of EGFP from cells transfected with either pEGFP or pEGFD-HD. HeLa cells were transfected with the indicated DNA, fixed, and visualized by confocal microscopy at 6 h after transfection.

two consensus sequences for N-linked glycosylation (NXS/T) at positions 2249 and 2252 (indicated by asterisks in Fig. 6A). If the hydrophobic amino acids in the HD are membrane-spanning sequences, these asparagine residues would be lumenal and available for modification. To determine if aspargine-2249 and -2252 were targeted for N-linked glycosylation, we mutated these residues to alanine (individually or as a double mutant), expressed the proteins with the vaccinia virus T7 expression system, and analyzed the products by SDS-PAGE. We found that PLpro-HD-N2249A and PLpro-HD-N2252A migrated more quickly in the gel than wild-type PLpro-HD (Fig. 6C, lanes 1 to 3) and that the double mutant migrated faster than each single mutant (Fig. 6C, lane 4).

To confirm that these differences in migration were due to differences in glycosylation, we treated PLpro-HD with endoglycosidase H to remove N-linked glycosylation and analyzed the products by SDS-PAGE. We found that PLpro-HD treated with endoglycosidase H migrated more quickly than the untreated protein (Fig. 6C, compare lanes 5 and 6), confirming that PLpro-HD is modified by N-linked glycosylation. Thus, the HD contains transmembrane sequences that are important for PLpro-mediated processing at the nsp3/4 cleavage site and that may serve to direct and anchor nsp3 and the associated replication complex to intracellular membranes. Future studies will be directed to resolving the glycosylated and unglycosylated forms of the 213-kDa nsp3 protein from SARS coronavirus-infected cells to confirm the membrane association and glycosylation of the native protein.

To determine if the HD can target a protein to intracellular membranes, we generated a reporter construct with eukaryotic green fluorescence protein (EGFP). We cloned the HD in-frame with the C-terminal end of EGFP and designated the plasmid pEGFP-HD. pEGFP and pEGFP-HD DNAs were transfected into HeLa cells, and the subcellular localization of the protein product was visualized by confocal microscopy (Fig. 6D). As expected, EGFP is detected throughout the cell, in both the cytoplasm and nucleus. In contrast, EGFP-HD is excluded from the nucleus and localizes in perinuclear patches consistent with membrane association. These results indicate that the HD may be a signal sequence that directs proteins to membranes. Similar studies were performed to identify an internal signal sequence in the hepatitis C virus polymerase (NS5B) protein (26). Future studies will be aimed at characterizing the putative coronavirus internal signal sequence that resides in nsp3.

DISCUSSION

In this study, we identified SARS coronavirus amino-terminal replicase products nsp1, nsp2, and nsp3 and characterized the PLpro activity that processes these products from the replicase polyprotein. We identified the replicase products by immunoprecipitation with specific antisera and used confocal microscopy to show that these replicase products colocalize with newly synthesized viral RNA in punctate, perinuclear patches in the cytoplasm of SARS coronavirus-infected cells. These results confirm the predicted role of nonstructural proteins as components of the SARS coronavirus replication complex. We found that nsp1, nsp2, and nsp3 are all processed from the replicase polyprotein by the PLpro domain that resides in nsp3.

This domain had been termed PL2pro because of its homology with other coronavirus PL2pro domains (26), but we found that the SARS coronavirus papain-like protease domain has activity consistent with both PL1pro and PL2pro and therefore designate it PLpro.

We established trans-cleavage assays to characterize SARS coronavirus PLpro activity and found that PLpro is sufficient to process the nsp1/2 and nsp2/3 sites but that the downstream hydrophobic domain is required for PLpro-mediated processing at the nsp3/4 cleavage site. We show that the hydrophobic domain sequence is glycosylated, that it mediates membrane association, and that it can act as a signal sequence to target EGFP to intracellular membranes. The hydrophobic domain may be important for directing and anchoring the replicase products to intracellular membranes where the replication complex is assembled. The development of trans-cleavage assays and the characterization of PLpro activity are important for future studies aimed at identifying antiviral drugs that will block the proteolytic processing of the replicase polyprotein, which is required for viral RNA synthesis (14).

The proteolytic processing map for the SARS coronavirus replicase polyprotein was generated by comparison of the SARS coronavirus sequence to other well-characterized coronaviruses (28, 30). Although the overall amino acid identify between SARS coronavirus and other coronaviruses is only ≈40% (20, 24), the positions and sequences of the protease cleavage sites are highly conserved. The identification of SARS coronavirus replicase products nsp1, nsp2, and nsp3 reported here confirms the accuracy of the predictions. Currently, the function of these nonstructural proteins is not known. However, biochemical and colocalization studies of a murine coronavirus indicate that these nonstructural proteins are part of a membrane-associated replication complex (5, 7).

Our confocal microscopy studies show that these SARS coronavirus replicase intermediates and/or products colocalize with newly synthesized viral RNA in punctate, perinuclear sites (Fig. 3). The punctate, perinuclear localization pattern is consistent with what has been seen for both coronaviruses and arteriviruses which have been shown to assemble double-membrane vesicles that are the sites of viral RNA synthesis (5, 7, 22). Indeed, double-membrane vesicles have been detected in SARS coronavirus-infected cells (6), and studies are ongoing to determine the role of each SARS coronavirus nonstructural protein in the assembly and function of double-membrane vesicles.

PLpro domains are conserved in all coronaviruses sequenced to date (reviewed in Ziebuhr et al. [34]). The murine coronavirus mouse hepatitis virus and human coronavirus 229E encode two PLpro domains, termed PL1pro and PL2pro and PLP1 and PLP2, respectively. For these viruses, PL1pro has been shown to process the nsp1/2 and nsp2/3 sites (2–4, 9, 10). For mouse hepatitis virus, PLP2 (also termed PL2pro) was shown to be responsible for processing the downstream nsp3/4 site (12, 13). For human coronavirus 229E, both PL1pro and PL2pro can process the nsp2/3 site in vitro, but it is unclear if PL1pro and PL2pro have redundant functions during viral replication (35). Infectious bronchitis virus of chickens encodes only one active PLpro domain, which processes one cleavage site upstream of the protease domain and one cleavage site downstream of the protease domain (18, 19).

Our studies showed that we can use *trans*-cleavage assays to assess SARS coronavirus PLpro activity. We found that SARS coronavirus PLpro cleaves the replicase polyprotein at the three predicted sites but with different kinetics and cofactors. The reason for the differences in processing activity is currently unclear, but we speculate that differential processing may be important for establishing a functional replication complex. For example, the NSP2-3 intermediate may have a role in the assembly of the replication complex that is independent of the nsp2 and nsp3 products. The *trans*-cleavage assay will be useful for determining the minimal domain required for PLpro activity and for identifying sequences that affect the kinetics of processing at the nsp1/nsp2 and nsp2/nsp3 cleavage sites.

Although the PLpro domain is sufficient for processing the upstream cleavage sites, we found that it is not able to process the downstream nsp3/4 cleavage site. Processing at the downstream cleavage site required expression of PLpro-HD (Fig. 5). The hydrophobic domain is conserved in all coronaviruses replicase sequences (32) and may play an important role in the assembly of the viral replication complex. We hypothesize that the SARS coronavirus replicase polyprotein becomes membrane-associated by the insertion of the hydrophobic domain into intracellular membranes. The hydrophobic domain contains stretches of predominantly hydrophobic amino acids and a lumenal domain that is modified by N-linked glycosylation. The insertion of PLpro-HD into intracellular membranes may allow colocalization of the protease and the cleavage site for processing. Our studies indicate that SARS coronavirus PLpro activity can be anchored to intracellular membranes and process a membrane-associated substrate.

The role of proteolytic processing in the assembly and function of the coronavirus replication complex is currently unclear. However, the recent development of a system that generates a complete cDNA clone of SARS coronavirus (33) will allow researchers to assess the role of proteolytic processing in viral RNA synthesis. Specific mutations in the proteases and cleavage sites can be introduced into the SARS coronavirus cDNA clone, and viral RNA can be synthesized and tested for its ability to replicate in transfected cells. These studies will allow us to identify the sequences and processing steps that are critical for the assembly and function of the SARS coronavirus replication complex. A detailed understanding of the structure and function of the SARS coronavirus proteases will provide critical information for the design of antiviral drugs that block viral replication and pathogenesis.

REFERENCES

1. **Anand, K., J. Ziebuhr, P. Wadhwani, J. R. Mesters, and R. Hilgenfeld.** 2003. Coronavirus main proteinase (3CLpro) structure: basis for design of anti-SARS drugs. Science **300:**1763–1767.

2. **Baker, S. C., C. K. Shieh, L. H. Soe, M. F. Chang, D. M. Vannier, and M. M. Lai.** 1989. Identification of a domain required for autoproteolytic cleavage of murine coronavirus gene A polyprotein. J. Virol. **63:**3693–3699.

3. **Bonilla, P. J., S. A. Hughes, J. D. Pinon, and S. R. Weiss.** 1995. Characterization of the leader papain-like proteinase of MHV-A59: identification of a new in vitro cleavage site. Virology **209:**489–497.

4. **Bonilla, P. J., S. A. Hughes, and S. R. Weiss.** 1997. Characterization of a second cleavage site and demonstration of activity in *trans* by the papain-like proteinase of the murine coronavirus mouse hepatitis virus strain A59. J. Virol. **71:**900–909.

5. **Brockway, S. M., C. T. Clay, X. T. Lu, and M. R. Denison.** 2003. Characterization of the expression, intracellular localization, and replication complex association of the putative mouse hepatitis virus RNA-dependent RNA polymerase. J. Virol. **77:**10515–10527.

6. **Goldsmith, C. S., K. M. Tatti, T. G. Ksiazek, P. E. Rollin, J. A. Comer, W. W. Lee, P. A. Rota, B. Bankamp, W. J. Bellini, and S. R. Zaki.** 2004. Ultrastructural characterization of SARS coronavirus. Emerg. Infect. Dis. **10:**320–326.

7. **Gosert, R., A. Kanjanahaluethai, D. Egger, K. Bienz, and S. C. Baker.** 2002. RNA replication of mouse hepatitis virus takes place at double-membrane vesicles. J. Virol. **76:**3697–3708.

8. **Gray, J.** 1999. Assays for virus infection, p. 84. *In* J. Cann (ed.), Virus culture: a practical approach. Oxford University Press Inc., New York, N.Y.

9. **Herold, J., A. E. Gorbalenya, V. Thiel, B. Schelle, and S. G. Siddell.** 1998. Proteolytic processing at the amino terminus of human coronavirus 229E gene 1-encoded polyproteins: identification of a papain-like proteinase and its substrate. J. Virol. **72:**910–918.

10. **Herold, J., S. G. Siddell, and A. E. Gorbalenya.** 1999. A human RNA viral cysteine proteinase that depends upon a unique Zn^{2+}-binding finger connecting the two domains of a papain-like fold. J. Biol. Chem. **274:**14918–14925.

11. **Ivanov, K. A., V. Thiel, J. C. Dobbe, Y. van der Meer, E. J. Snijder, and J. Ziebuhr.** 2004. Multiple enzymatic activities associated with severe acute respiratory syndrome coronavirus helicase. J. Virol. **78:**5619–5632.

12. **Kanjanahaluethai, A., and S. C. Baker.** 2000. Identification of mouse hepatitis virus papain-like proteinase 2 activity. J. Virol. **74:**7911–7921.

13. **Kanjanahaluethai, A., D. Jukneliene, and S. C. Baker.** 2003. Identification of the murine coronavirus MP1 cleavage site recognized by papain-like proteinase 2. J. Virol. **77:**7376–7382.

14. **Kim, J. C., R. A. Spence, P. F. Currier, X. Lu, and M. R. Denison.** 1995. Coronavirus protein processing and RNA synthesis is inhibited by the cysteine proteinase inhibitor E64d. Virology **208:**1–8.

15. **Ksiazek, T. G., D. Erdman, C. S. Goldsmith, S. R. Zaki, T. Peret, S. Emery, S. Tong, C. Urbani, J. A. Comer, W. Lim, P. E. Rollin, S. F. Dowell, A. E. Ling, C. D. Humphrey, W. J. Shieh, J. Guarner, C. D. Paddock, P. Rota, B. Fields, J. DeRisi, J. Y. Yang, N. Cox, J. M. Hughes, J. W. LeDuc, W. J. Bellini, and L. J. Anderson.** 2003. A novel coronavirus associated with severe acute respiratory syndrome. N. Engl. J. Med. **348:**1953–1966.

16. **Kuiken, T., R. A. Fouchier, M. Schutten, G. F. Rimmelzwaan, G. van Amerongen, D. van Riel, J. D. Laman, T. de Jong, G. van Doornum, W. Lim, A. E. Ling, P. K. Chan, J. S. Tam, M. C. Zambon, R. Gopal, C. Drosten, S. van der Werf, N. Escriou, J. C. Manuguerra, K. Stohr, J. S. Peiris, and A. D. Osterhaus.** 2003. Newly discovered coronavirus as the primary cause of severe acute respiratory syndrome. Lancet **362:**263–270.

17. **Lai, M. M. C., and K. V. Holmes.** 2001. Coronaviridae: the viruses and their replication, p. 1163–1185. *In* D. M. Knipe and P. M. Howley (ed.), Fields Virology. Lippincott Williams and Wilkins, Philadelphia, Pa.

18. **Lim, K. P., and D. X. Liu.** 1998. Characterization of the two overlapping papain-like proteinase domains encoded in gene 1 of the coronavirus infectious bronchitis virus and determination of the C-terminal cleavage site of an 87-kDa protein. Virology **245:**303–312.

19. **Lim, K. P., L. F. Ng, and D. X. Liu.** 2000. Identification of a novel cleavage activity of the first papain-like proteinase domain encoded by open reading frame 1a of the coronavirus Avian infectious bronchitis virus and characterization of the cleavage products. J. Virol. **74:**1674–1685.

20. **Marra, M. A., S. J. Jones, C. R. Astell, R. A. Holt, A. Brooks-Wilson, Y. S. Butterfield, J. Khattra, J. K. Asano, S. A. Barber, S. Y. Chan, A. Cloutier, S. M. Coughlin, D. Freeman, N. Girn, O. L. Griffith, S. R. Leach, M. Mayo, H. McDonald, S. B. Montgomery, P. K. Pandoh, A. S. Petrescu, A. G. Robertson, J. E. Schein, A. Siddiqui, D. E. Smailus, J. M. Stott, G. S. Yang, F. Plummer, A. Andonov, H. Artsob, N. Bastien, K. Bernard, T. F. Booth, D. Bowness, M. Drebot, L. Fernando, R. Flick, M. Garbutt, M. Gray, A. Grolla, S. Jones, H. Feldmann, A. Meyers, A. Kabani, Y. Li, S. Normand, U. Stroher, G. A. Tipples, S. Tyler, R. Vogrig, D. Ward, B. Watson, R. C. Brunham, M. Krajden, M. Petric, D. M. Skowronski, C. Upton, and R. L. Roper.** 2003. The genome sequence of the SARS-associated coronavirus. Science **300:**1399–1404.

21. **Ng, M. L., S. H. Tan, E. E. See, E. E. Ooi, and A. E. Ling.** 2003. Proliferative growth of SARS coronavirus in Vero E6 cells. J. Gen. Virol. **84:**3291–3303.

22. **Pedersen, K. W., Y. van der Meer, N. Roos, and E. J. Snijder.** 1999. Open reading frame 1a-encoded subunits of the arterivirus replicase induce endoplasmic reticulum-derived double-membrane vesicles which carry the viral replication complex. J. Virol. **73:**2016–2026.

23. **Peiris, J. S. M., S. T. Lai, L. L. M. Poon, Y. Guan, L. Y. C. Yam, W. Lim, J. Nicholls, W. K. S. Yee, W. W. Yan, M. T. Cheung, V. C. C. Cheng, K. H. Chan, D. N. C. Tsang, R. W. H. Yung, T. K. Ng, and K. Y. Yuen.** 2003. Coronavirus as a possible cause of severe acute respiratory syndrome. Lancet **361:**1319–1325.

24. **Rota, P. A., M. S. Oberste, S. S. Monroe, W. A. Nix, R. Campagnoli, J. P. Icenogle, S. Penaranda, B. Bankamp, K. Maher, M. H. Chen, S. Tong, A. Tamin, L. Lowe, M. Frace, J. L. DeRisi, Q. Chen, D. Wang, D. D. Erdman, T. C. Peret, C. Burns, T. G. Ksiazek, P. E. Rollin, A. Sanchez, S. Liffick, B. Holloway, J. Limor, K. McCaustland, M. Olsen-Rassmussen, R. Fouchier, S. Gunther, A. D. Osterhaus, C. Drosten, M. A. Pallansch, L. J. Anderson, and W. J. Bellini.** 2003. Characterization of a novel coronavirus associated with severe acute respiratory syndrome. Science **300:**1394–1399.

25. **Schiller, J. J., A. Kanjanahaluethai, and S. C. Baker.** 1998. Processing of the coronavirus MHV-JHM polymerase polyprotein: identification of precursors and proteolytic products spanning 400 kilodaltons of ORF1a. Virology **242:** 288–302.

26. **Schmidt-Mende, J., E. Bieck, T. Hugle, F. Penin, C. M. Rice, H. E. Blum, and D. Moradpour.** 2001. Determinants for membrane association of the hepatitis C virus RNA-dependent RNA polymerase. J. Biol. Chem. **276:**44052–44063.

27. **Shi, S. T., J. J. Schiller, A. Kanjanahaluethai, S. C. Baker, J. W. Oh, and M. M. Lai.** 1999. Colocalization and membrane association of murine hepatitis virus gene 1 products and de novo-synthesized viral RNA in infected cells. J. Virol. **73:**5957–5969.

28. **Snijder, E. J., P. J. Bredenbeek, J. C. Dobbe, V. Thiel, J. Ziebuhr, L. L. Poon, Y. Guan, M. Rozanov, W. J. Spaan, and A. E. Gorbalenya.** 2003. Unique and conserved features of genome and proteome of SARS-coronavirus, an early split-off from the coronavirus group 2 lineage. J. Mol. Biol. **331:**991–1004.

29. **Stadler, K., V. Masignani, M. Eickmann, S. Becker, S. Abrignani, H. D. Klenk, and R. Rappuoli.** 2003. SARS—beginning to understand a new virus. Nat. Rev. Microbiol. **1:**209–218.

30. **Thiel, V., K. A. Ivanov, A. Putics, T. Hertzig, B. Schelle, S. Bayer, B. Weissbrich, E. J. Snijder, H. Rabenau, H. W. Doerr, A. E. Gorbalenya, and J. Ziebuhr.** 2003. Mechanisms and enzymes involved in SARS coronavirus genome expression. J. Gen. Virol. **84:**2305–2315.

31. **Wang, D., A. Urisman, Y. T. Liu, M. Springer, T. G. Ksiazek, D. D. Erdman, E. R. Mardis, M. Hickenbotham, V. Magrini, J. Eldred, J. P. Latreille, R. K. Wilson, D. Ganem, and J. L. DeRisi.** 2003. Viral discovery and sequence recovery using DNA microarrays. Public Library Sci. Biol. **1:**257–260.

32. **Yang, H., M. Yang, Y. Ding, Y. Liu, Z. Lou, Z. Zhou, L. Sun, L. Mo, S. Ye, H. Pang, G. F. Gao, K. Anand, M. Bartlam, R. Hilgenfeld, and Z. Rao.** 2003. The crystal structures of severe acute respiratory syndrome virus main protease and its complex with an inhibitor. Proc. Natl. Acad. Sci. USA **100:** 13190–13195.

33. **Yount, B., K. M. Curtis, E. A. Fritz, L. E. Hensley, P. B. Jahrling, E. Prentice, M. R. Denison, T. W. Geisbert, and R. S. Baric.** 2003. Reverse genetics with a full-length infectious cDNA of severe acute respiratory syndrome coronavirus. Proc. Natl. Acad. Sci. USA **100:**12995–13000.

34. **Ziebuhr, J., E. J. Snijder, and A. E. Gorbalenya.** 2000. Virus-encoded proteinases and proteolytic processing in the Nidovirales. J. Gen. Virol. **81:**853–879.

35. **Ziebuhr, J., V. Thiel, and A. E. Gorbalenya.** 2001. The autocatalytic release of a putative RNA virus transcription factor from its polyprotein precursor involves two paralogous papain-like proteases that cleave the same peptide bond. J. Biol. Chem. **276:**33220–33232.